electronics

MDPI

Article

Physical Features of High-Density Barium–Tungstate–Phosphate (BTP) Glasses: Elastic Moduli, and Gamma Transmission Factors

Hesham M. H. Zakaly [1,2,*], Huseyin O. Tekin [3,4], Yasser S. Rammah [5], Shams A. M. Issa [2,6], Ali Hamed Alomari [7], Fatema T. Ali [8], Duygu Sen Baykal [9], Wiam Elshami [3], D. E. Abulyazied [6,10], Ghada ALMisned [11], A. M. A. Mostafa [12] and Antoaneta Ene [13,*]

1 Institute of Physics and Technology, Ural Federal University, 620002 Ekaterinburg, Russia
2 Physics Department, Faculty of Science, Al-Azhar University, Assiut 71524, Egypt
3 Department of Medical Diagnostic Imaging, College of Health Sciences, University of Sharjah, Sharjah 27272, United Arab Emirates
4 Faculty of Engineering and Natural Sciences, Computer Engineering Department, Istinye University, 34396 Istanbul, Turkey
5 Department of Physics, Faculty of Science, Menoufia University, Shebin El-Koom, Menoufia 32511, Egypt
6 Physics Department, Faculty of Science, University of Tabuk, P.O. Box 741, Tabuk 47512, Saudi Arabia
7 Physics Department, Al-Qunfudah University College, Umm Al-Qura University, P.O. Box 715, Al Qunfudah 28821, Saudi Arabia
8 Center for Advanced Materials Research, Research Institute of Sciences and Engineering, University of Sharjah, Sharjah 27272, United Arab Emirates
9 Vocational School of Health Sciences, Medical Imaging Techniques, Istanbul Kent University, 34433 Istanbul, Turkey
10 Polymer Lab, Department of Petrochemical, Egyptian Petroleum Research Institute, Nasr City, Cairo 11421, Egypt
11 Department of Physics, College of Science, Princess Nourah Bint Abdulrahman University, P.O. Box 84428, Riyadh 11671, Saudi Arabia
12 Physics Department, College of Science, Jouf University, P.O. Box 2014, Sakaka 72341, Saudi Arabia
13 INPOLDE Research Center, Department of Chemistry, Physics and Environment, Faculty of Sciences and Environment, Dunarea de Jos University of Galati, 47 Domneasca Street, 800008 Galati, Romania
* Correspondence: h.m.zakaly@gmail.com (H.M.H.Z.); antoaneta.ne@ugal.ro (A.E.)

Citation: Zakaly, H.M.H.; Tekin, H.O.; Rammah, Y.S.; Issa, S.A.M.; Alomari, A.H.; Ali, F.T.; Baykal, D.S.; Elshami, W.; Abulyazied, D.E.; ALMisned, G.; et al. Physical Features of High-Density Barium–Tungstate–Phosphate (BTP) Glasses: Elastic Moduli, and Gamma Transmission Factors. *Electronics* **2022**, *11*, 4095. https://doi.org/10.3390/electronics11244095

Academic Editors: Wiesław Leonski and Lucas Lamata

Received: 9 October 2022
Accepted: 1 December 2022
Published: 8 December 2022

Publisher's Note: MDPI stays neutral with regard to jurisdictional claims in published maps and institutional affiliations.

Abstract: We present elastic moduli, gamma radiation attenuation characteristics, and transmission factor of barium–tungstate–phosphate (BTP) glasses with the chemical formula (60-y)BaO-yWO_3-40P_2O_5, where y = 10 (S1)–40 (S4) in steps of 10 mole%. Different types of mathematical and simulation approaches, such as the Makishima–Mackenzie model, the Monte Carlo method, and the online Phy-X/PSD software, are utilized in terms of determining these parameters. The total packing density (V_t) is enriched from 0.607 to 0.627, while the total energy dissociation (G_t) is enriched by increasing the WO_3 content (from 52.2 (kJ/cm^3). In the investigated glasses, increasing tungstate trioxide (WO_3) contribution enhanced Young's, shear, bulk, and longitudinal moduli. Moreover, Poisson's ratio is improved by increasing the WO_3 content in the BTP glasses. The 20BaO-40WO_3-40P_2O_5 sample possessed the highest values of both linear (μ) and mass attenuation (μm) coefficients, i.e., (μ, μm)$_{S4}$ > (μ, μm)$_{S3}$ > (μ, μm)$_{S2}$ > (μ, μm)$_{S1}$. Moreover, the 20BaO-40WO_3-40P_2O_5 sample had the lowest values of half (HVL) and tenth (TVL) layers, i.e., (half, tenth)$_{S4}$ < (half, tenth)$_{S3}$ < (half, tenth)$_{S2}$ < (half, tenth)$_{S1}$. The effective atomic number (Z_{eff}) of the studied glasses has the same behavior as μ and μm. Finally, the 20BaO-40WO_3-40P_2O_5 is reported with the minimum values of transmission factor (TF) for all the BTP investigated at a thickness of 3 cm. In conclusion, the sample with composition 20BaO-40WO_3-40P_2O_5 which has the maximum WO_3 reinforcement may be a beneficial glass sample, along with its advanced mechanical and gamma ray shielding properties.

Keywords: BTP glasses; elastic moduli; Phy-X/PSD; radiation shielding; MCNPX

1. Introduction

Radiology service has undergone enormous growth in terms of radiation procedures and personnel. It is widely known that most healthcare patients will stop by the radiology department. Besides computed tomography, the use of interventional procedures has risen in recent years. Nurses, surgeons, including orthopedics gemmologists, and other physicians are frequently present during radiation examinations [1,2]. Radiation workers and students in the medical field are exposed to unavoidable occupational radiation exposure [3–5]. However, radiation medical workers showed an understanding of the importance of radiation protection, but there is variation in the practice of radiation protection [6,7], and poor practice of using radiation protection tools was demonstrated [8,9]. The available lead shields are limited as they are challenging to use and carry due to heaviness and thickness. Therefore, medical radiation workers are not wearing lead shielding during procedures [10]. However, lead is the most popular shielding material; it has a few downsides that must be considered. Heaviness and musculoskeletal issues make it tough to use. Furthermore, it is a hazardous substance and raises biological and environmental problems [11]. Consequently, new shielding materials are needed to address the shortcomings of the lead apron and enhance radiation attenuation efficiency. Meanwhile, several investigations have been carried out to provide enhanced radiation protection techniques for the synthesizing and development of new shielding materials [12,13]. Recent investigations have stressed that glass shields [14–20] are one of the most ambitious materials that might be used as an alternative for conventional materials that are disadvantaged in certain ways. Researchers in the literature [21–30] are particularly interested in glass structures because of the high permeability they provide and the exceptional mechanical properties they possess. It has also been pushed to a position where it is emphasized and developed in daily radiation safety practice because of the non-toxic nature of glasses and the chemical compositions that may be synthesized at high densities. Glassy structures may be created using a wide range of chemical compositions. The unique optical, mechanical, structural, and radiation attenuation characteristics of each structure are enhanced because of this process.

Phosphate glasses have gained increased interest due to their potential applications in a variety of industrial and scientific fields, including radiation shielding, along with excellent physical characteristics, including high thermal expansion coefficients, low melting and softening temperatures, and high ultra-violet and far infrared transmission [31–33].

Barium oxide (BaO) is considered as a network modifier oxide in the glass structure [34]. Glasses containing phosphorus as a glass former and alkali and alkaline earth metals as modifiers have been found to be stable [35].

Tungsten trioxide (WO_3) is one of the oxides that, in a variety of P_2O_5 compositions, may combine to produce glass; these kinds of glass have high optical basicity and high refractive index [36–38]. A form of oxide known as WO_3 is introduced into glass compositions at different rates to boost the radiation-shielding properties of the glass. In this case, the relevance is derived from the monotonic impact that these WO_3 additive rates have had on the radiation shielding properties [36–38].

Since BaO has a relatively high density, we hypothesized that replacing barium oxide (BaO) with tungsten trioxide (WO3) would change the mechanical and gamma ray attenuation characteristics.

A group of $BaO–WO_3–P_2O_5$ glasses [38] with varying compositions was characterized to investigate the changes in radiation attenuation, mechanical, and gamma ray transmission characteristics that occur in conjunction with altering WO_3 additive ratios in a group of $BaO–WO_3–P_2O_5$ glasses [38]. These properties of four glass samples with varied structural features and WO_3 additive ratios were investigated systematically in this study. Accordingly, their elastic, mechanical, and radiation attenuation characteristics were extensively investigated.

In addition to providing a substantial contribution to the glass literature, the results of this work may contribute to a greater understanding of the role of WO_3 in the production and design of high-density glassy radiation shields.

2. Materials and Methods

2.1. High-Density Barium–Tungstate–Phosphate (BTP) Glasses

Through the current study, four barium–tungstate–phosphate glasses with the chemical formula (60-y)BaO-yWO_3-40P_2O_5, where y = 10–40 in steps of 10 mol%, were chosen [38]. The investigated glasses have the following criteria: Table 1.

(60-10)BaO-10WO_3-40P_2O_5 (**S1**) with density (ϱ = 4.21 g/cm^3 and molar volume (V_m = 37.2 cm^3/mol)).

(60-20)BaO-20WO_3-40P_2O_5 (**S2**) with density (ϱ = 4.18 g/cm^3 and molar volume (V_m = 39.4 cm^3/mol)).

(60-30)BaO-30WO_3-40P_2O_5 (**S3**) with density (ϱ = 4.31 g/cm^3 and molar volume (V_m = 38.3 cm^3/mol)).

(60-40)BaO-40WO_3-40P_2O_5 (**S4**) with density (ϱ = 4.50 g/cm^3 and molar volume (V_m = 40.00 cm^3/mol)), Table 1.

Table 1. Includes the sample codes, elemental weight fractions, density, and molar volume of the studied glasses.

Samples Code	Elemental Compositions (wt%)				Composition (mol%)			Density, ϱ (g/cm^3) ± 0.01 [38]	Molar Volume, V_m (cm^3/mol) ± 0.01 [38]
	O	P	Ba	W	BaO	P_2O_5	WO_3		
S1	0.286015	0.158207	0.438403	0.117376	50	40	10	4.21	37.2
S2	0.291817	0.150655	0.333981	0.223546	40	40	20	4.18	39.4
S3	0.297091	0.143792	0.239075	0.320043	30	40	30	4.31	38.3
S4	0.301905	0.137526	0.152438	0.40813	20	40	40	4.5	40

2.2. Elastic Moduli of Barium–Tungstate–Phosphate (BTP) Glasses

The mechanical elastic moduli of the proposed barium–tungstate–phosphate (S1–S4) glasses, including Young's modulus (E^{MM}), bulk modulus (K^{MM}), shear modulus (S^{MM}), longitudinal modulus (L^{MM}), and Poisson's ratio (σ^{MM}), have been investigated. This investigation has been achieved via the conventional Makishima–Mackenzie [39–43]. This model mainly depends on the functions of both total packing density (V_t) and the total dissociation energy per unit volume (G_t) of the chemical bonds in the glass samples, as [39–43]:

$$V_t = \left(\frac{1}{V_m}\right)\sum_i (V_i x_i) \quad (1)$$

$$G_t = \sum_i (G_i x_i) \ \ (\mathrm{kJ}/cm^3) \quad (2)$$

where, (V_i) in Equation (1) and (G_i) in Equation (2) are the ionic radius and the average strength of each oxide in the glass composition for each sample. Via the values of (V_t) and (G_t), all elastic moduli can be given as [33–37]:

$$E^{MM} = 2V_t G_t \quad (3)$$

$$K^{MM} = 1.2V_t E^{MM} \quad (4)$$

$$S^{MM} = \frac{(3E^{MM}K^{MM})}{(9K^{MM}-E^{MM})} \quad (5)$$

$$L^{MM} = K^{MM} + \frac{4}{3}S^{MM} \quad (6)$$

Moreover, Poisson's ratio (σ^{MM}) can be calculated as [39–43]:

$$\sigma^{MM} = \left(\frac{E^{MM}}{2G^{MM}}\right) - 1 \quad (7)$$

2.3. Radiation Shielding Parameters and Transmission Factors (TFs) of Barium–Tungstate–Phosphate (BTP) Glasses

As a matter of fact, structural alterations in materials affect the lowering rate of energetic photons. Depending on the approach utilized, these alterations might be analyzed utilizing parameters or computed by assessing the complete material. Radiation transmission is characterized as a ratio between the intensity of the input radiation and output radiation, or secondary radiation, which is formed as a consequence of attenuation in the medium [44]. Monte Carlo simulation software, MCNPX [45], and a theoretical program, Phy-X/PSD [46], were utilized to calculate the gamma ray shielding properties and transmission factors (TFs) of the investigated glasses, respectively. For several well-known radioisotopes, such as ^{67}Ga, ^{57}Co, ^{111}In, ^{133}Ba and ^{99}Tc, there were individual TF values of each glass sample for various glass thicknesses. To quantify primary and secondary gamma radiation intensity, two detection zones (F4 Tally Mesh) [45] were set up in front of and behind the glass shield. Figure 1 depicts the MCNPX simulation setup for calculating the gamma ray transmission factor. Creating an adequate input file for a Monte Carlo simulation is the first step in creating a simulation environment that can be used for the investigation. We used a Lenovo® ThinkStation-P620/30E0008QUS Workstation (Beijing, China) as our main processor throughout the Monte Carlo simulation.

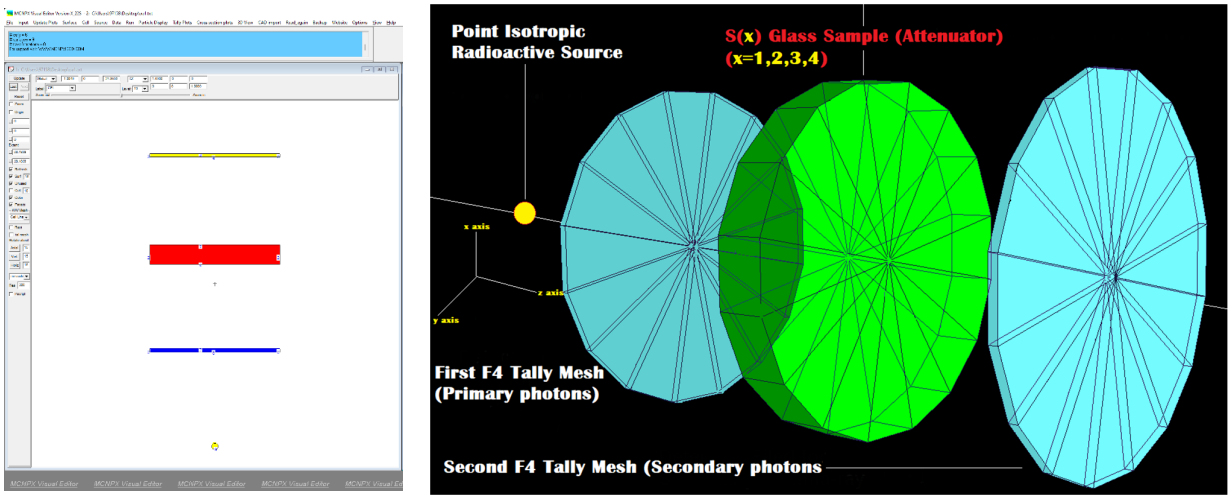

(**a**) (**b**)

Figure 1. (**a**) A 2-D view of designed MCNPX simulation setup; (**b**) 3-D illustration of designed MCNPX setup (2-D and 3-D views are obtained from MCNPX Visual Editor VisedX22S).

3. Results and Discussions

3.1. Elastic Moduli of Barium–Tungstate–Phosphate Glasses

Relations (1) and (2) are used to calculate the values of the total packing density (V_t) and the total dissociation energy (G_t) of the suggested samples (S1–S4). These calculations have been performed via the (V_i) and (G_i) values of each glass oxide P_2O_5, BaO, and WO_3, as collected in Table 2. Figure 2 and Table 3 show the changing of G_t and V_t parameters as a function of tungstate trioxide (WO_3) concentration in mol% of the S1–S4 glasses. Figure 2 shows that the value of (V_t) increases from 0.589 for the WO3-free sample (S1) to 0.605 for the WO3-rich sample. This can be explained as a result of increasing content of WO3

at the expense of P2O5, which energizes the glass structure. It can be further noticed that increasing WO3 beyond 10 mol% in the investigated glass network causes the overall packing density (V_t) to decrease slightly. This might be due to the peak of the largest band for W-O bond vibrations falling to a lower wavenumber. If we look deeply at Table 3 and Figure 3, we find that the (V_t) enhances from 0.607 to 0.627 for S1 and S4 glasses. The improving trend of (V_t) may be due to the larger ionic radius of WO3 compared to that of BaO. By the same trend, the (G_t) factory enhances from 52.2 to 60.36 (kJ/cm^3) for S1 and S4 glasses, thus the trend of the (G_t) may be due to the WO_3 having the highest dissociation energy (67.8 kJ/cm^3) compared to BaO (40.6 kJ/cm^3) and P_2O_5 (62.8 kJ/cm^3). The obtained values of (V_t) and (G_t) were applied in relation (3), and then Young`s elastic modulus (E^{MM}) was calculated for all (S1–S4) glasses. In the next step, relation (4) was used to calculate the bulk modulus (K^{MM}) of the suggested glasses. Then, relations (5) and (6) were used to calculate both shear modulus (S^{MM}) and longitudinal modulus (L^{MM}), respectively. The obtained values of (E^{MM}), (K^{MM}), (S^{MM}) and (L^{MM}) are tabulated in Table 3 and plotted in Figure 3**.** As shown, the values of the (E^{MM}) were improved with an enhancement of tungstate trioxide (WO_3) concentration in glasses; the (E^{MM}) values varied from 63.426 GPa to 75.631 GPa for S1 and S4, respectively. This improvement may be related to the increase in the total dissociation energy and packing density with increasing in WO_3 concentration. Furthermore, as shown in Figure 3, the obtained values of the (K^{MM}) were enhanced from 46.239 Gpa to 56.859 GPa for S1 and S4 glasses. The values of the (S^{MM}) were improved from 24.944 GPa to 29.582 GPa, while values of the (L_{MM}) were increased from 79.414 GPa to 96.204 Gpa. In addition, via relation (7), Poisson's ratio (σ^{MM}) of the investigated glasses was examined and its values were tabulated in Table 3 and graphed in Figure 4. The values of (σ^{MM}) were improved from 0.271 to 0.278 for S1 and S4 glasses. The trend of the elastic moduli of the current glasses may be related to the decrease in the amount of non-bridging oxygen (NBO) and vacancies as the WO3 concentration in glasses increases [39–43].

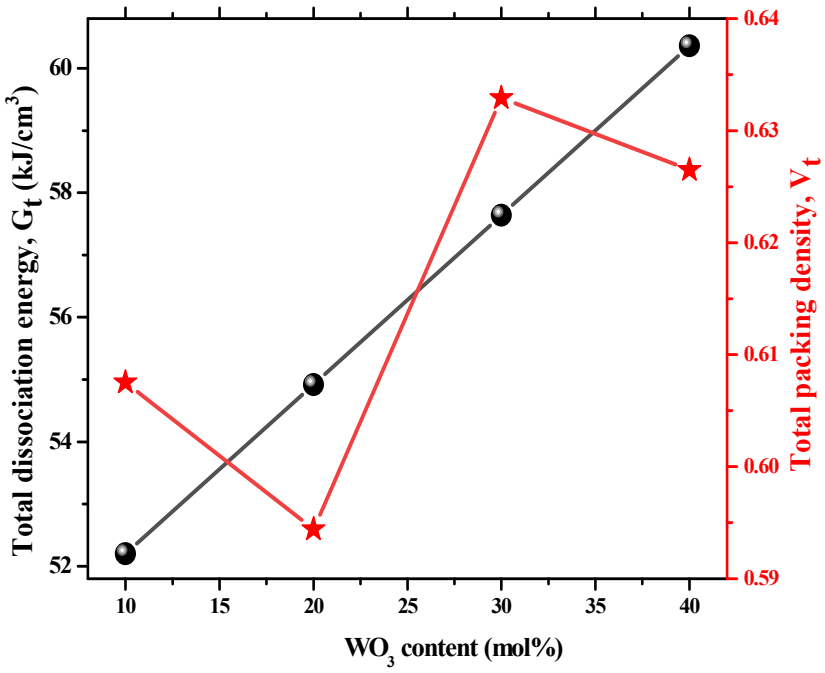

Figure 2. Variation of G_t and V_t as a function of WO_3 content (mol%) of the investigated glasses.

Table 2. Packing density factor (V_i), and dissociation/bond energy per unit volume (G_i) of the oxides BaO, WO_3, and P_2O_5.

Oxide	V_i (cm^3/mol) [37,38]	G_i (kJ/cm^3) [37,38]
BaO	13.1	40.6
WO_3	21.3	67.8
P_2O_5	34.8	62.8

Table 3. Total ionic packing density (V_t), total dissociation energy (G_t), Young's modulus (E^{MM}), bulk modulus (K^{MM}), shear modulus (S^{MM}), longitudinal modulus (L^{MM}) and Poisson's ratio (σ^{MM}) based on the Makishima–Mackenzie model of the studied glasses. The x_i is the mole fraction of component i of an oxide glass and V_m is the molar volume of the glass samples.

Parameters and Elastic Moduli	S1	S2	S3	S4
$V_t = \left(\frac{1}{V_m}\right)\sum_i(V_i x_i) \pm 0.001$	**0.607**	**0.594**	**0.633**	**0.627**
$G_t = \sum_i(G_i x_i) \pm 0.001$ (kJ/cm^3)	**52.2**	**54.92**	**57.64**	**60.36**
$E^{MM} = 2V_t G_t \pm 0.01$ (GPa)	**63.426**	**65.291**	**72.961**	**75.631**
$K^{MM} = 1.2V_t E_{MM} \pm 0.001$ (GPa)	**46.239**	**46.572**	**55.412**	**56.859**
$S^{MM} = \frac{(3E_{MM}K_{MM})}{(9K_{MM}-E_{MM})} \pm 0.001$ Gpa)	**24.944**	**25.779**	**28.488**	**29.582**
$L^{MM} = K_{MM} + \frac{4}{3}S_{MM} \pm 0.001$ (Gpa)	**79.414**	**80.858**	**93.301**	**96.204**
$\sigma^{MM} = \left(\frac{E_{MM}}{2G_{MM}}\right) - 1 \pm 0.001$ (GPa)	**0.271**	**0.266**	**0.281**	**0.278**

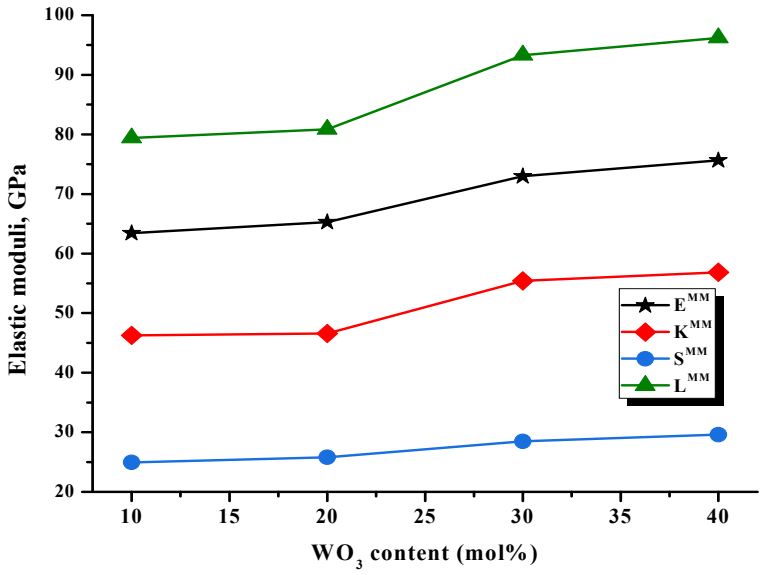

Figure 3. Variation of elastic moduli as a function of WO_3 content mol% of the investigated glasses.

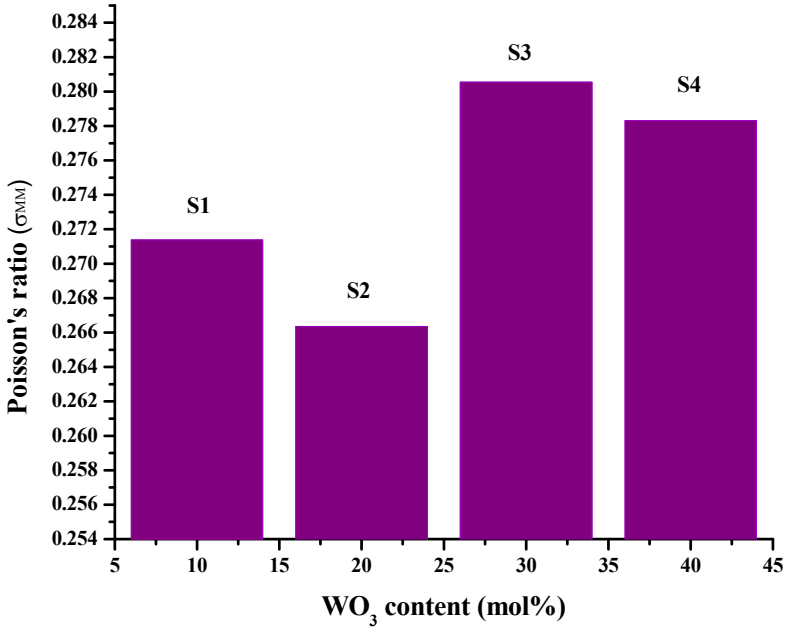

Figure 4. Variation of Poisson's ratio as a function of WO_3 content (mol%) of the investigated glasses.

3.2. Radiation Shielding Features of Barium–Tungstate–Phosphate (BTP) Glasses

Another part of characterizing the explored glass group in this work was the measurement of the gamma ray shielding capabilities and transmission factors (TFs) of four individual glass samples (S1, S2, S3, and S4). The density of materials has a substantial effect on their gamma ray shielding characteristics owing to the increased possibility of interaction between the material and the gamma ray [47–50]. On the other hand, it is critical to observe the density variation of glassy materials to have a better understanding of the influence of integrated elements on the glass composition's fluctuation. Figure 5 illustrates the variance in material densities of the tested glasses, S1, S2, S3 and S4. Between samples S1 and S4, there was a rise in glass density. The above-mentioned density increase may be explained by the fact that the WO_3 additive rate in the S1 sample has been continuously rising with each consecutive sample, leading to the maximum amount of WO_3 in S4 sample. As a consequence of the continuous WO_3 inclusion having the most impact on the S4 sample, the maximum glass density was determined to be 4.5 g/cm^3. Furthermore, it was clearly observed that the net density difference between the S1 and S4 samples is 0.29 g/cm^3. This variation may be explained by the elemental weight percent influence of W rising from 11 to 40 wt. percent in the glass composition, resulting in a net rise of glass density of 0.29 g/cm^3. The initial phase of the recent investigation was the determination of linear attenuation coefficient (μ), which is a fundamental property of a candidate shielding material that can be determined for various photon energy values from low to high (MeV). The variation of the μ values regarding different energy values is illustrated in Figure 6 as a function of utilized photon energy values from 0.015 to 15 MeV. When an incoming photon interacts with the corresponding shielding matter, it might undergo several special interactions (i.e., photoelectric effect, Compton scattering, and pair production), with some having priority over others. For instance, the photoelectric effect (PE) is the most prominent of the few types of interactions found in the low-energy zone. As seen in Figure 6, linear attenuation coefficients have begun to decrease dramatically in the low-photon energy zone. This significantly declined trend in low energy is the result of the

supremacy of the PEA procedure, which is α Z^5 and (1/E3.^{5}). Accordingly, the S4 sample had the highest linear attenuation coefficients in comparison to all other glass materials, namely S1, S2, and S3, examined. The majority of the cause for this circumstance is due to the maximum WO_3 contribution described above, as well as the WO_3 additive's direct effect on the glass' density. Compton scattering predominates in the medium energies, which are α Z and (1/E), whereas pair production prevails at high-photon energies, which are α Z^2. Figure 6 shows that the low-energy region has sharp discontinuities near element absorption edges. The sharp peaks are ascribed to K-absorption edges at 0.035 MeV and 0.06 MeV. The appearance of these edges is due to the presence of Ba and W, respectively. Following the determination of μ values in a variety of photon energies, another critical gamma ray shielding parameter, which is known as the mass attenuation coefficient (μ_m), was also determined for the same photon energy range. Figure 7 demonstrates the relationship between increasing gamma ray energy and corresponding μ_m values (cm^2/g) for all S1–S4 samples. We noticed a remarkable similarity in behavioral attitudes, such as linear attenuation coefficients, over a broad variety of gamma ray energy ranges, including low-, intermediate- as well as high-energy photons. Compared to other examined glass samples, the S4 sample had the greatest μ_m values of all photon energies studied. One potential explanation for this circumstance is that the highest elemental concentration of WO_3 in the structure of S4 altered the behavior of mass attenuation coefficients, owing to the compound's higher atomic number. Owing to the certain substitutions that have been implemented in the glassy matrix, this has resulted in a drop in the number of low-atomic-number elements, resulting in an increase in the incorporation of high-atomic-number elements, such as W. It broadly recognized that calculating shielding properties of the candidate materials may be performed in different useful ways, each of which enables the user to input a range of various types of data that may be useful in actual applications. Half value layer (HVL) as a shielding parameter may be considered as a part of the decision process not only for superiority but also for engineering aspects of the manufacturing process of the shielding materials. Therefore, the term half value layer clearly stresses the attenuation produced by shielding materials engaging with gamma rays on an atomic scale. The HVL measurements are very valuable for determining the needed shield thickness of a material at which gamma ray intensity is reduced by half. For that purpose, any shielding material capable of halving the strength of gamma radiation at thin layers is deemed an ideal shield for utilization purposes. In the recent investigation, we evaluated the HVL values for glass samples throughout an energy range of 0.015–15 MeV as attenuation coefficients. As shown in Figure 8, the observed behaviors of the investigated specimens varied substantially as the photon energy increased and, accordingly, HVL thickness increased. The half value widths are smallest in the region of low-photon energy, but they increase correspondingly as energy levels increase. The HVL values needed for the low-energy photons in all the glass samples studied are very thin, owing to the weak penetration properties of those photons. However, required HVL thickness values increased dramatically in the zone of high energy, as shown in Figure 8. According to our calculations, the S4 sample with the maximum WO_3 contribution exhibits the lowest HVL values across the entire photon energy range from low to high. Calculating the effective atomic number (Z_{eff}) of a compound may be a valuable technique for monitoring overall variations in the gamma ray attenuation qualities as a function of the atomic number variation in complex structures. In other words, the primary reason for calculating this value is because the structural changes generated by chemical alterations to the material define the atomic number that will be effective in the photon energy responsible. Figure 9 depicts the changes in Z_{eff} values as a function of photon energy. As previously stated, S4 has the highest WO_3 incorporation, which provided some considerable effects on previously described shielding metrics, such as linear and mass attenuation coefficients, as well as half-value layer values. The increase in overall atomic number with the incorporation of W (Z = 74) in the glass matrix was shown to result in a large rise in Z_{eff} in the lowest energy range. According to our findings, the S4 with the highest mass attenuation coefficients

exhibits the highest Zeff values for the relevant photon energy. As a final stage of the characterization process, the gamma ray transmission factor (TF) values for the investigated glass samples were determined for several commonly used radioisotope energies, including ^{67}Ga, ^{57}Co, ^{111}In, ^{133}Ba, ^{201}Tl, ^{99}Tc, ^{51}Cr, ^{131}I, ^{58}Co, ^{137}Cs, and ^{60}Co. For samples with varied glass thicknesses, TF factors were determined. Figure 10 depicts the transmission factors (TFs) of studied glasses as a function of used radioisotope energy (MeV) at various glass thicknesses. The calculated transmission factors rise in proportion to the increasing radioisotope energy (from 0.0086 MeV to 1.3326 MeV). Our initial findings strongly indicated that, regardless of composition, the TF values in the low-energy zone were the lowest for glass samples of all thicknesses. Glass samples of varying thicknesses display a spectrum of reactions after being exposed to 0.1 MeV gamma rays. Maximum attenuation (also known as the lowest TF) values were recorded for all glass materials studied at a thickness of 3 cm. Due to the fact that the attenuation capacity of any shielding material is exactly proportional to its thickness, this situation may be attributed to the fact that increasing the shield thickness increases the attenuation potential of gamma rays reaching the shielding material's structure. Furthermore, we compared the attenuation abilities of the analyzed glasses at 0.5 cm, 1.5 cm, 2.5 cm, and 3.0 cm glass thicknesses. Figure 11 illustrates various glass thicknesses as a function of the radioisotope energy (MeV) utilized to calculate the transmission factor (TF). As can be seen, all thicknesses display a decrease in TF values as the quantity of incoming gamma ray energy rises. When exposed to high-energy gamma rays, the S4 sample has shown exceptional transmission characteristics across all glass thicknesses utilized at the final stage of the TF characterization phase.

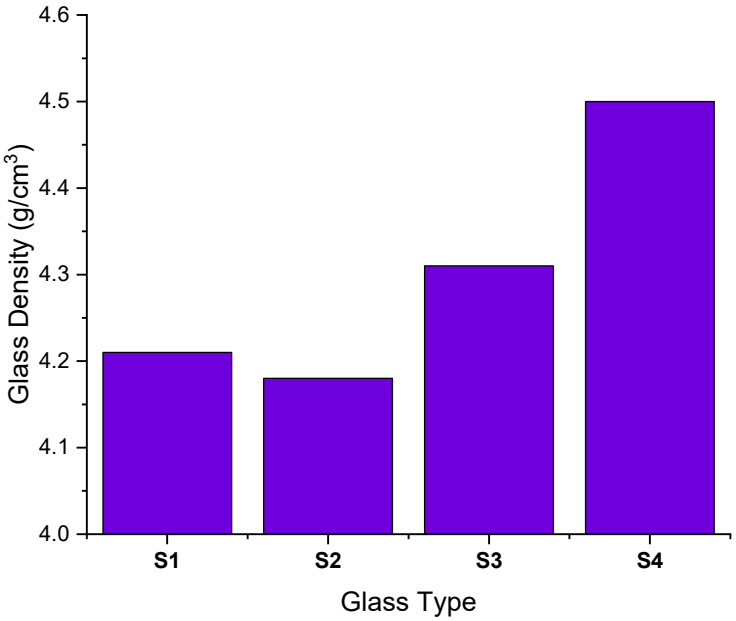

Figure 5. Variation of glass densities.

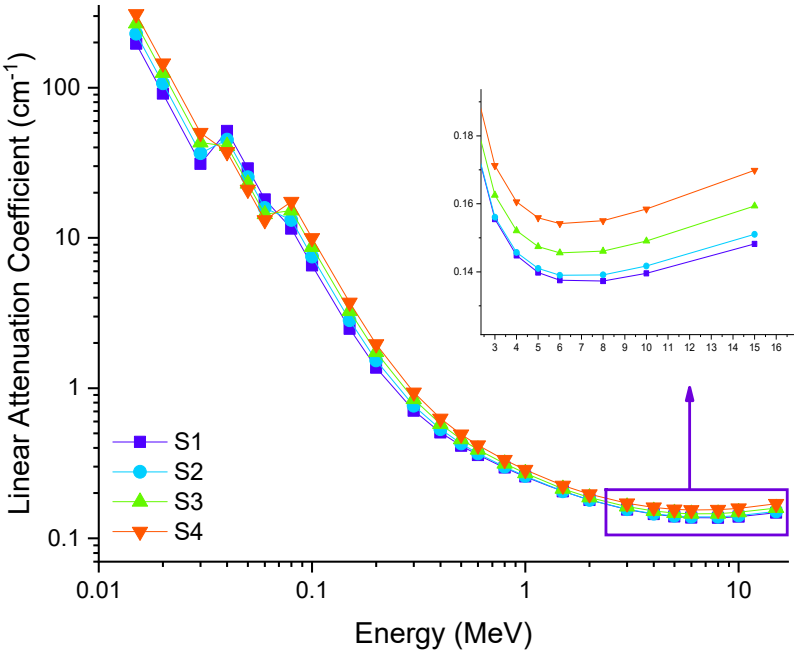

Figure 6. Variations of linear attenuation coefficient (cm^{-1}) with photon energy (MeV) for all S1–S4 glasses.

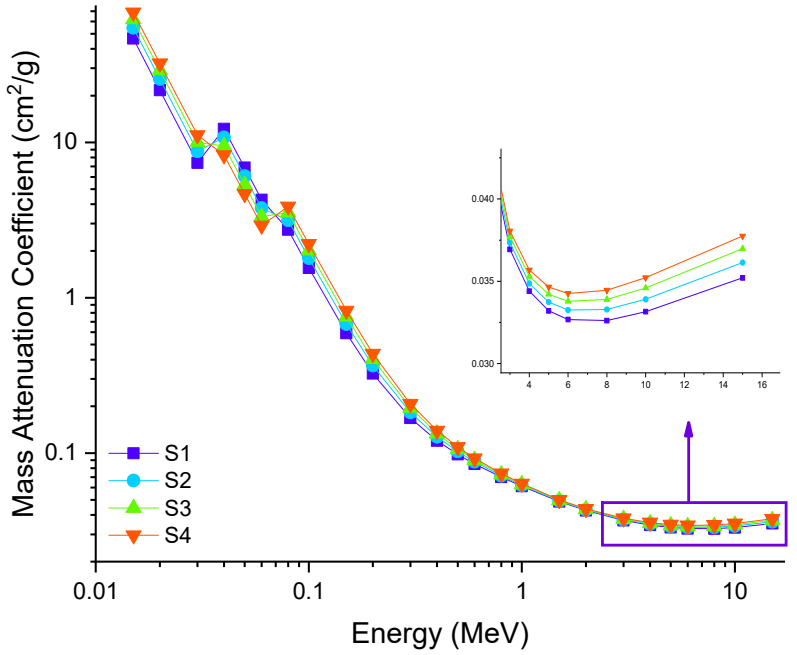

Figure 7. Variation of mass attenuation coefficients (cm^2/g) with photon energy (MeV) for all S1–S4 glasses.

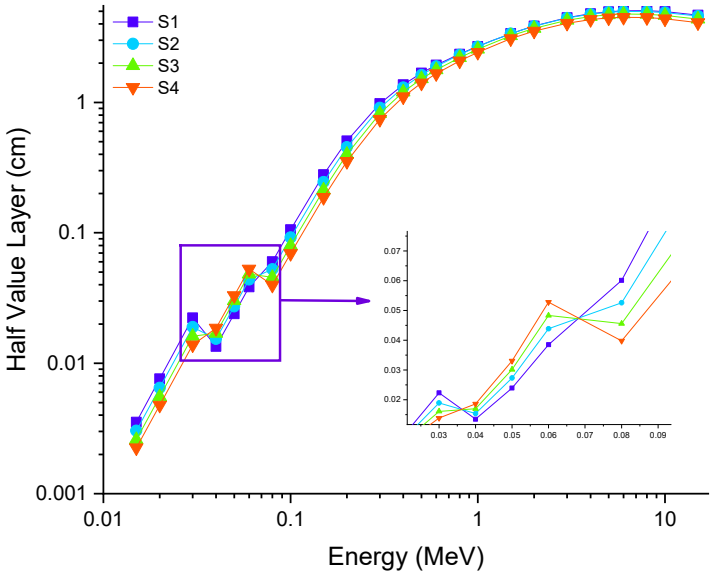

Figure 8. Variation of half value layer (cm) with photon energy (MeV) for all S1–S4 glasses.

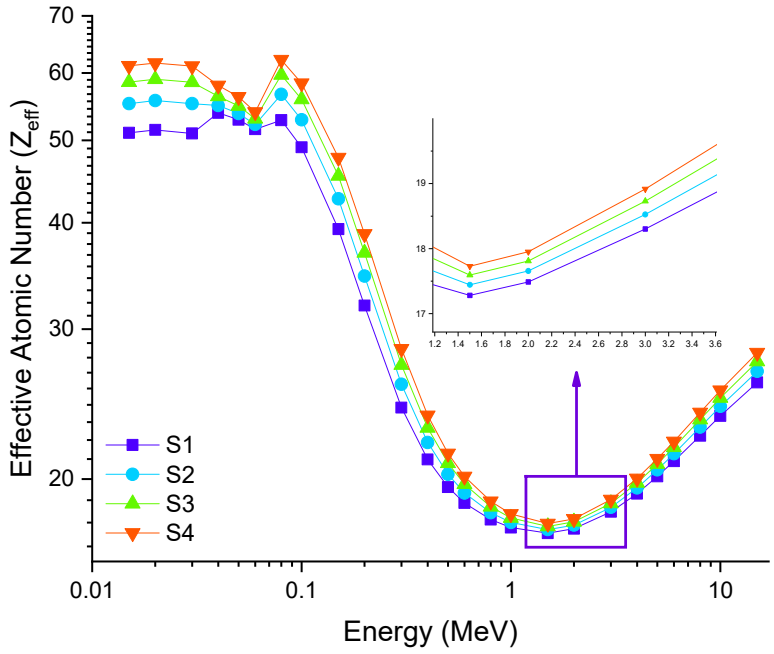

Figure 9. Variations of effective atomic number (Z_{eff}) with photon energy (MeV) for all S1–S4 glasses.

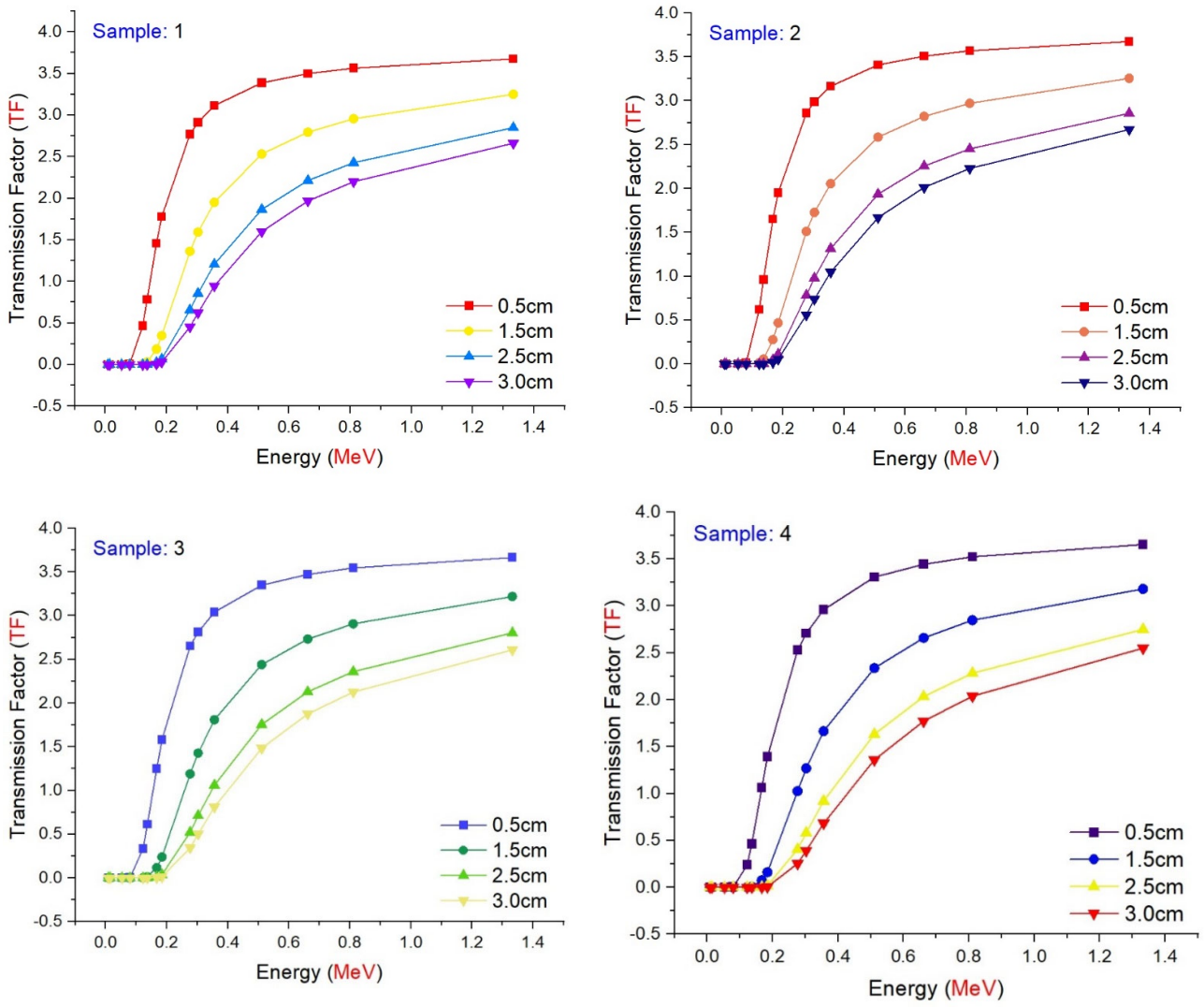

Figure 10. Transmission factors (TFs) of investigated glasses as a function of used radioisotope energy (MeV) at different glass thicknesses.

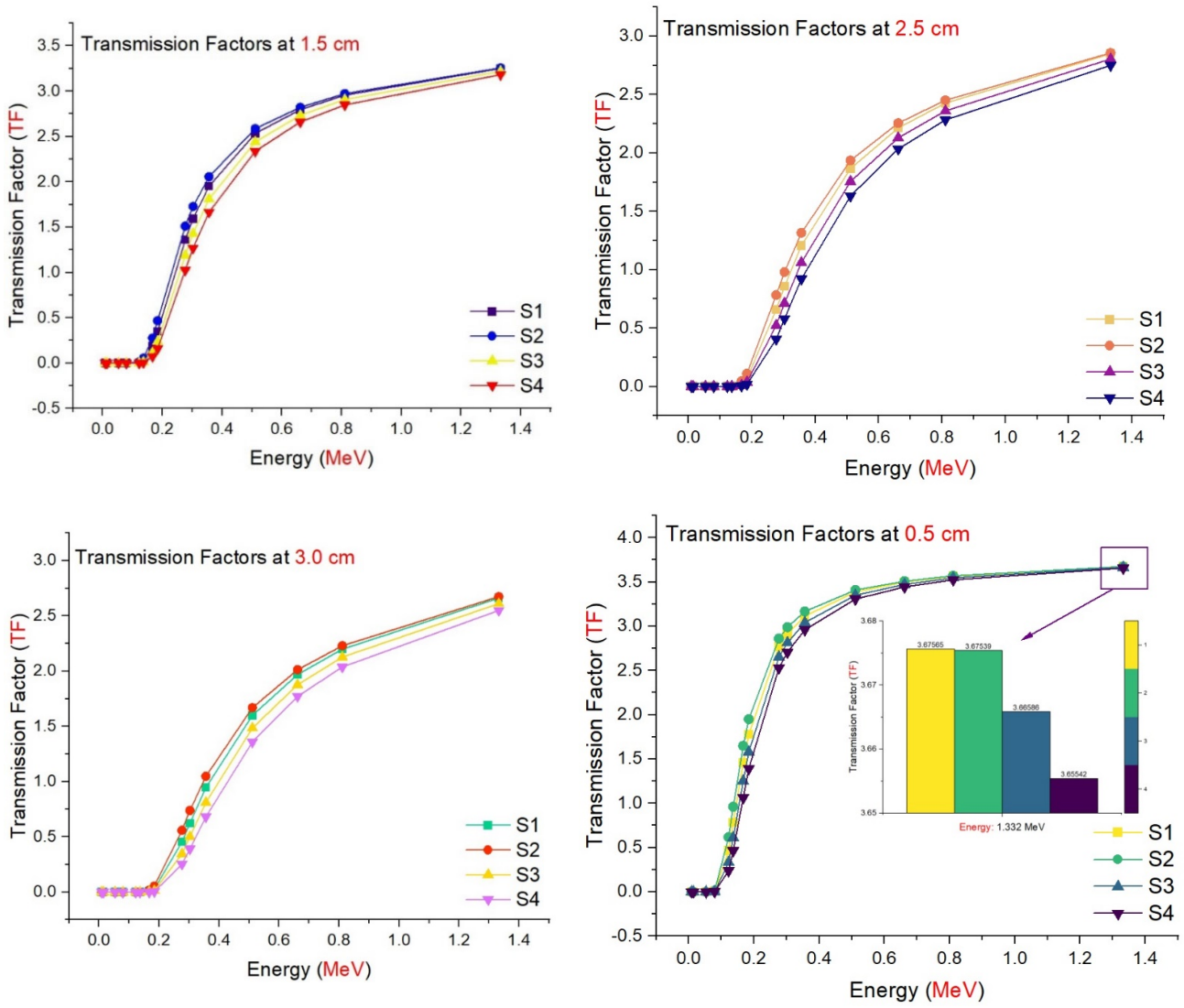

Figure 11. Comparison of the transmission factors (TFs) as a function of used radioisotope energy (MeV) for different glass thicknesses.

4. Conclusions

Four samples of barium–tungstate–phosphate (BTP) glasses with the chemical formula (60-y)BaO-yWO_3-40P_2O_5, where y = 10–40 in steps of 10 mol%, have been selected. Makishima–Mackenzie model, Monte Carlo code, and the newly online Phy-X/PSD software were applied to investigate the elastic moduli, gamma radiation attenuation characteristics, and transmission factors of the BTP glasses. According to our findings, the total packing density (V_t) was enriched from 0.607 to 0.627 for S1 and S4 samples. Similarly, the total energy dissociation (G_t) of the tested glasses was enriched by increasing the WO_3 content (from 52.2 (kJ/cm^3) for S1 glasses to 60.36 (*kJ*/cm^3) for S4 glasses). By increasing the tungstate trioxide (WO_3) in the investigated glasses, Young's, shear, bulk, and longitudinal moduli were enhanced. Furthermore, Poisson's ratio was improved by increasing the WO_3 content in the BTP glasses. The S4 sample possessed the highest values of both linear (μ) and mass attenuation (μ_m) coefficients. However, (μ, μ_m)$_{S4}$ > (μ, μ_m)$_{S3}$ > (μ, μ_m)$_{S2}$ > (μ, μ_m)$_{S1}$. Aside from this, the S4 sample had the lowest values of half (HVL) and tenth (TVL) layers in comparison to the other examined glasses. Therefore, (half, tenth)$_{S4}$ < (half, tenth)$_{S3}$ < (half, tenth)$_{S2}$ < (half, tenth)$_{S1}$. The effective atomic number (Z_{eff}) of the studied

glasses has the same behavior as LAC and MAC. Finally, S4 achieved the minimum transmission factor (TF) values for all the BTP investigated at a thickness of 3 cm. However, the S4 sample exhibited superior radiation shielding characteristics.

Author Contributions: Conceptualization, H.O.T., H.M.H.Z., A.M.A.M., G.A. and S.A.M.I.; methodology, F.T.A. and H.O.T.; software, D.S.B., A.H.A., H.M.H.Z. and A.E.; validation, S.A.M.I., A.M.A.M., D.S.B., D.E.A., W.E., Y.S.R. and A.E.; formal analysis, H.M.H.Z., and F.T.A.; investigation, H.O.T., W.E., and G.A.; resources, F.T.A. and D.S.B.; data curation, S.A.M.I., A.H.A. and A.E.; writing—original draft preparation, Y.S.R., D.E.A., H.O.T., D.E.A., F.T.A. and A.E.; writing—review and editing, H.M.H.Z., S.I, A.M.A.M., A.H.A. and A.E.; visualization, W.E. and A.E.; supervision, H.M.H.Z., W.E., Y.S.R. and D.S.B.; project administration, H.O.T., A.E., Y.S.R. and S.A.M.I.; funding acquisition A.E. (The APC was funded by "Dunarea de Jos" University of Galati, Romania). All authors have read and agreed to the published version of the manuscript.

Funding: Deanship of Scientific Research at Umm Al-Qura University supported this work by Grant Code: (22UQU4300274DSR01).

Data Availability Statement: The data presented in this study are available on request from the corresponding author.

Acknowledgments: The authors would like to thank the Deanship of Scientific Research at the Umm Al-Qura University for supporting this work. The APC was covered by "Dunarea de Jos" University of Galati, Romania

Conflicts of Interest: The authors declare no conflict of interest.

References

1. Ahn, S.; Kim, W.Y.; Lim, K.S.; Ryoo, S.M.; Sohn, C.H.; Seo, D.W.; Kwak, M.K.; Yoon, J.C. Advanced radiology utilization in a tertiary care emergency department from 2001 to 2010. *PLoS ONE* **2014**, *9*, e112650.
2. Elshami, W.; Abuzaid, M.; Pekkarinen, A.; Kortesniemi, M. Estimation of occupational radiation exposure for medical workers in radiology and cardiology in the united arab emirates: Nine hospitals experience. *Radiat. Prot. Dosim.* **2020**, *189*, 466–474.
3. Abuzaid, M.M.; Elshami, W.; Steelman, C. Measurements of radiation exposure of radiography students during their clinical training using thermoluminescent dosimetry. *Radiat. Prot. Dosim.* **2017**, *179*, 244–247.
4. Gurjar, O.P.; Jha, V.K.; Sharma, S.D. Radiation dose to radiotherapy technologists due to induced activity in high energy medical electron linear accelerators. *Radiat. Prot. Environ.* **2014**, *37*, 25.
5. Elshami, W.; Abuzaid, M.; Piersson, A.D.; Mira, O.; AbdelHamid, M.; Zheng, X.; Kawooya, M.G. Occupational dose and radiation protection practice in UAE: A retrospective cross-sectional cohort study (2002–2016). *Radiat. Prot. Dosim.* **2019**, *187*, 426–437.
6. Abuzaid, M.M.; Elshami, W.; Shawki, M.; Salama, D. Assessment of compliance to radiation safety and protection at the radiology department. *Int. J. Radiat. Res.* **2019**, *17*, 439–446.
7. Abuzaid, M.M.; Elshami, W.; Hasan, H. Knowledge and adherence to radiation protection among healthcare workers at operation theater. *Asian J. Sci. Res.* **2018**, *12*, 54–59.
8. NG, S.E.; SA, F. Assessment of awareness and practice of ionizing radiation protection procedures among exposed health care workers. *Egypt. J. Occup. Med.* **2020**, *44*, 529–544.
9. Geletu, G.M.; Abiko, F.; Sahlu, S. Implementation of a radiation protection system at four hospitals in Ethiopia. *arXiv* **2019**, arXiv:1905.07271.
10. Zuguchi, M.; Chida, K.; Taura, M.; Inaba, Y.; Ebata, A.; Yamada, S. Usefulness of non-lead aprons in radiation protection for physicians performing interventional procedures. *Radiat. Prot. Dosim.* **2008**, *131*, 531–534.
11. Scuderi, G.J.; Brusovanik, G.V.; Campbell, D.R.; Henry, R.P.; Kwon, B.; Vaccaro, A.R. Evaluation of non–lead-based protective radiological material in spinal surgery. *Spine J.* **2006**, *6*, 577–582.
12. Elshami, W.; Tekin, H.O.; Al-Buriahi, M.S.; Hegazy, H.H.; Abuzaid, M.M.; Issa, S.A.; Zaid, M.H.M.; Sidek, H.A.A.; Matori, K.; Zakaly, H.M. Developed selenium dioxide-based ceramics for advanced shielding applications: Au2O3 impact on nuclear radiation attenuation. *Results Phys.* **2021**, *24*, 104099.
13. Deliormanlı, A.M.; Ensoylu, M.; Issa, S.A.; Elshami, W.; Al-Baradi, A.M.; Al-Buriahi, M.S.; Tekin, H.O. WS2/bioactive glass composites: Fabrication, structural, mechanical and radiation attenuation properties. *Ceram. Int.* **2021**, *47*, 29739–29747.
14. ALMisned, G.; Elshami, W.; Issa, S.A.; Susoy, G.; Zakaly, H.M.; Algethami, M.; Rammah, Y.S.; Ene, A.; Al-Ghamdi, S.A.; Ibraheem, A.A.; et al. Enhancement of gamma-ray shielding properties in cobalt-doped heavy metal borate glasses: The role of lanthanum oxide reinforcement. *Materials* **2021**, *14*, 7703.
15. Saudi, H.A.; Tekin, H.O.; Zakaly, H.M.H.; Issa, S.A.M.; Susoy, G.; Zhukovsky, M. The impact of samarium (III) oxide on structural, optical and radiation shielding properties of thallium-borate glasses: Experimental and numerical investigation. *Opt. Mater.* **2021**, *114*, 110948. https://doi.org/10.1016/j.optmat.2021.110948.

16. Tekin, H.O.; Issa, S.A.M.; Ahmed, E.M.; Rammah, Y.S. Lithium-fluoro borotellurite glasses: Nonlinear optical, mechanical, characteristics and gamma radiation protection characteristics. *Radiat. Phys. Chem.* **2022**, *190*, 109819. https://doi.org/10.1016/j.radphyschem.2021.109819.
17. Kilic, G.; Ilik, E.; Issa, S.A.M.; Issa, B.; Al-Buriahi, M.S.; Issever, U.G.; Zakaly, H.M.H.; Tekin, H.O. Ytterbium (III) oxide reinforced novel TeO_2–B_2O_3–V_2O_5 glass system: Synthesis and optical, structural, physical and thermal properties. *Ceram. Int.* **2021**, *47*, 18517–18531. https://doi.org/10.1016/j.ceramint.2021.03.175.
18. Saudi, H.; Zakaly, H.M.; Issa, S.A.; Tekin, H.; Hessien, M.; Rammah, Y.; Henaish, A. Fabrication, FTIR, physical characteristics and photon shielding efficacy of CeO_2 /sand reinforced borate glasses: Experimental and simulation studies. *Radiat. Phys. Chem.* **2021**, *191*, 109837. https://doi.org/10.1016/j.radphyschem.2021.109837.
19. Alalawi, A.; Al-Buriahi, M.S.; Rammah, Y.S. Radiation shielding properties of PNCKM bioactive glasses at nuclear medicine energies. *Ceram. Int.* **2020**, *46*, 15027–15033. https://doi.org/10.1016/j.ceramint.2020.03.033.
20. Abouhaswa, A.S.; El-Agawany, F.I.; Ahmed, E.M.; Rammah, Y.S. Optical, magnetic characteristics, and nuclear radiation shielding capacity of newly synthesized barium boro-vanadate glasses: B_2O_3–BaF_2–Na_2O–V_2O_5. *Radiat. Phys. Chem.* **2021**, *192*, 109922. https://doi.org/10.1016/j.radphyschem.2021.109922.
21. Issa, S.A.M.; Rashad, M.; Zakaly, H.M.H.; Tekin, H.O.; Abouhaswa, A.S. Nb_2O_5-Li_2O-Bi_2O_3-B_2O_3 novel glassy system: Evaluation of optical, mechanical, and gamma shielding parameters. *J. Mater. Sci. Mater. Electron.* **2020**, *31*, 22039–22056. https://doi.org/10.1007/s10854-020-04707-7.
22. Rammah, Y.; Olarinoye, I.; El-Agawany, F.; Ahmed, E.M.; Salem, W.M. Influence of Sm_2O_3 content on photon and fast neutron interaction parameters of zinc-tellurite glasses. *Radiat. Phys. Chem.* **2022**, *192*, 109914. https://doi.org/10.1016/j.radphyschem.2021.109914.
23. Rammah, Y.S.; El-Agawany, F.I.; Abdel Wahab, E.A.; Hessien, M.M.; Shaaban, K.S. Significant impact of V2O5 content on lead phosphor-arsenate glasses for mechanical and radiation shielding applications. *Radiat. Phys. Chem.* **2022**, *193*, 109956. https://doi.org/10.1016/j.radphyschem.2021.109956.
24. Tekin, H.O.; Issa, S.A.M.; Kilic, G.; Zakaly, H.M.H.; Tarhan, N.; Sidek, H.A.A.; Matori, K.A.; Zaid, M.H.M. A systematical characterization of TeO_2–V_2O_5 glass system using boron (Iii) oxide and neodymium (iii) oxide substitution: Resistance behaviors against ionizing radiation. *Appl. Sci.* **2021**, *11*, 3035. https://doi.org/10.3390/app11073035.
25. Rammah, Y.S.; Olarinoye, I.O.; El-Agawany, F.I.; El-Adawy, A.; Yousef, E. The impact of PbF2 on the ionizing radiation shielding competence and mechanical properties of TeO_2–PbF_2 glasses and glass-ceramics. *Ceram. Int.* **2020**, *47*, 2547–2556. https://doi.org/10.1016/j.ceramint.2020.09.100.
26. Rammah, Y.S.; Zakaly, H.M.H.; Issa, S.A.M.; Tekin, H.O.; Hessien, M.M.; Saudi, H.A.; Henaish, A.M.A. Fabrication, physical, structural, and optical investigation of cadmium lead-borate glasses doped with Nd3+ ions: An experimental study. *J. Mater. Sci. Mater. Electron.* **2021**, *33*, 1877–1887. https://doi.org/10.1007/s10854-021-07387-z.
27. Hegazy, H.H.; Al-Buriahi, M.S.; Alresheedi, F.; El-Agawany, F.I.; Sriwunkum, C.; Neffati, R.; Rammah, Y.S. Nuclear shielding properties of B_2O_3–Bi_2O_3–SrO glasses modified with Nd_2O_3: Theoretical and simulation studies. *Ceram. Int.* **2020**, *47*, 2772–2780. https://doi.org/10.1016/j.ceramint.2020.09.131.
28. Tekin, H.O.; ALMisned, G.; Susoy, G.; Ali, F.T.; Baykal, D.S.; Ene, A.; Issa, S.A.M.; Rammah, Y.S.; Zakaly, H.M.H. Transmission Factor (TF) Behavior of Bi_2O_3–TeO2–Na_2O–TiO_2–ZnO Glass System: A Monte Carlo Simulation Study. *Sustainability* **2022**, *14*, 2893. https://doi.org/10.3390/su14052893.
29. Zhang, B.; He, F.; Cao, X.; Wei, M.; Zheng, C.; Xie, J. The effect of TiO_2 and B_2O_3 on sintering behavior and crystallization behavior of SrO–BaO–B_2O_3–SiO_2 glass-ceramics. *Ceram. Int.* **2022**, *48*, 7013–7023.
30. Zhang, B.; He, F.; Cao, X.; Ren, H.; Yan, D.; Xie, J. Effect of SiO2/BaO ratio on sintering behavior, crystallization behavior, and properties of SrO–BaO–B_2O_3–SiO_2 glass-ceramics. *Ceram. Int.* **2021**, *47*, 19043–19051.
31. Agar, O.; Khattari, Z.Y.; Sayyed, M.I.; Tekin, H.O.; Al-Omari, S.; Maghrabi, M.; Zaid, M.H.M.; Kityk, I.V. Evaluation of the shielding parameters of alkaline earth based phosphate glasses using MCNPX code. *Results Phys.* **2018**, *12*, 101–106. https://doi.org/10.1016/J.RINP.2018.11.054.
32. Rammah, Y.S.; Kilic, G.; El-Mallawany, R.; Issever, U.G.; El-Agawany, F.I. Investigation of optical, physical, and gamma-ray shielding features of novel vanadyl boro-phosphate glasses. *J. Non-Cryst. Solids* **2020**, *533*, 119905. https://doi.org/10.1016/J.JNONCRYSOL.2020.119905.
33. Zakaly, H.M.H.; Saudi, H.A.; Issa, S.A.M.; Rashad, M.; Elazaka, A.I.; Tekin, H.O.; Saddeek, Y.B. Alteration of optical, structural, mechanical durability and nuclear radiation attenuation properties of barium borosilicate glasses through BaO reinforcement: Experimental and numerical analyses. *Ceram. Int.* **2021**, *47*, 5587–5596. https://doi.org/10.1016/j.ceramint.2020.10.143.
34. Doweidar, H.; El-Damrawi, G.; Agammy, E.F. El Structural correlations in BaO-PbO-B2O3 glasses as inferred from FTIR spectra. *Vib. Spectrosc.* **2014**, *73*, 90–96. https://doi.org/10.1016/j.vibspec.2014.05.003.
35. Sene, F.F.; Martinelli, J.R.; Gomes, L. Synthesis and characterization of niobium phosphate glasses containing barium and potassium. *Non-Cryst. Solids* **2004**, *348*, 30–37. https://doi.org/10.1016/J.JNONCRYSOL.2004.08.122.
36. Koudelka, L.; Šubčík, J.; Mošner, P.; Gregora, I.; Montagne, L.; Delevoye, L.; Gregora, I. Glass-forming ability and structure of glasses in ZnO-WO_3-P_2O_5 system. *Phys. Chem. Glasses Eur. J. Glass Sci. Technol. B* **2012**, *53*, 79–85.
37. Koudelka, L.; Rösslerová, I.; Mošner, P.; Černošek, Z.; Lissová, M.; Liška, M.; Montagne, L.; Delevoye, L. Structure and properties of lead tungstate-phosphate glasses. *Phys. Chem. Glasses Eur. J. Glass Sci. Technol. B* **2012**, *53*, 86–92.

38. Kalenda, P.; Koudelka, L.; Mošner, P.; Montagne, L.; Revel, B. Glass-forming ability and the structure of glasses in the BaO-WO_3-$P2O_5$ system. *J. Non-Cryst. Solids* **2020**, *541*, 120145.
39. Makishima, A.; Mackenzie, J.D. Direct Calculation of Young's Modulus of Glass. *J. Non-Cryst. Solids* **1973**, *12*, 35–45.
40. Inaba, S.; Fujino, Sh.; Morinaga, K. Young's Modulus and Compositional Parameters of Oxide Glasses. *J. Am. Ceram. Soc.* **1999**, *82*, 3501–3507.
41. Olarinoye, I.O.; El-Agawany, F.I.; El-Adawy, A.; Yousef, E.; Rammah, Y.S. Mechanical features, alpha particles, photon, proton, and neutron interaction parameters of TeO_2–$V2O_3$–MoO_3 semiconductor glasses. *Ceram. Int.* **2020**, *46*, 23134–23144.
42. Rammah, Y.S.; Olarinoye, I.O.; El-Agawany, F.I.; El-Adawy, A.; Gamal, A.; Yousef, E. Elastic moduli, photon, neutron, and proton shielding parameters of tellurite bismo-vanadate (TeO_2–V_2O_5–Bi_2O_3) semiconductor glasses. *Ceram. Int.* **2020**, *46*, 25440–25452.
43. Elkhoshkhany, N.; Syala, E.; Yousef, E. Concentration dependence of the elastic moduli, thermal properties, and non-isothermal kinetic parameters of Yb3+ doped multicomponent tellurite glass system. *Results Phys.* **2020**, *16*, 102876.
44. Almateri, M.; Agar, O.; Altunsoy, E.E.; Kilicoglu, O.; Sayyed, M.I.; Tekin, H.O. Photon and neutron shielding characteristics of samarium doped lead alumino borate glasses containing barium, lithium and zinc oxides determined at medical diagnostic energies. *Results Phys.* **2019**, *12*, 2123–2128. https://doi.org/10.1016/j.rinp.2019.01.094.
45. IAEA. *RSICC Computer Code Collection, MCNPX User's Manual Version 2.4.0. Monte Carlo N-Particle Transport Code System for Multiple and High Energy Applications*; IAEA: Vienna, Austria. 2004. Available online: https://inis.iaea.org/search/searchsinglerecord.aspx?recordsFor=SingleRecord&RN=39098954 (accessed on 1 October 2022).
46. Şakar, E.; Özpolat, Ö.F.; Alım, B.; Sayyed, M.I.; Kurudirek, M. Phy-X/PSD: Development of a user friendly online software for calculation of parameters relevant to radiation shielding and dosimetry. *Radiat. Phys. Chem.* **2019**, *166*, 108496. https://doi.org/10.1016/j.radphyschem.2019.108496.
47. Akkurt, I.; Tekin, H.O. Radiological Parameters for Bismuth Oxide Glasses Using Phy-X/PSD Software. *Emerg. Mater. Res.* **2020**, *9*, 1020–1027. https://doi.org/10.1680/jemmr.20.00209.
48. Ozge Kilicoglu, H.O. Tekin. Bioactive glasses and direct effect of increased K2O additive for nuclear shielding performance: A comparative investigation. *Ceram. Int.* **2019**, *46*, 1323–1333. https://doi.org/10.1016/j.ceramint.2019.09.095.
49. Lakshminarayana, G.; Kumar, A.; Tekin, H.; Issa, S.A.; Al-Buriahi, M.; Dong, M.; Lee, D.-E.; Yoon, J.; Park, T. Illustration of distinct nuclear radiation transmission factors combined with physical and elastic characteristics of barium boro-bismuthate glasses. *Results Phys.* **2021**, *31*, 105067. https://doi.org/10.1016/j.rinp.2021.105067.
50. El-Taher, A.; Zakaly, H.M.H.; Pyshkina, M.; Allam, E.A.; El-Sharkawy, R.M.; Mahmoud, M.E.; Abdel-Rahman, M.A.E. A comparative Study Between Fluka and Microshield Modeling Calculations to study the Radiation-Shielding of Nanoparticles and Plastic Waste composites. *Z. Fur Anorg. Und Allg. Chem.* **2021**, *647*, 1083–1090. https://doi.org/10.1002/zaac.202100062.